Non-Gaussian transport in strong plasma turbulence

S. V. Annibaldi
School of Cosmic Physics, Dublin Institute for Advanced Studies, 5 Merrion Square, Dublin 2, Republic of Ireland (Association Euratom/DCU)

G. Manfredi
Laboratoire de Physique des Milieux Ionisés, Université Henri Poincaré, BP239, 54506 Vandoeuvre-les-Nancy, France

R. O. Dendy
EURATOM/UKAEA Fusion Association, Culham Science Centre, Abingdon, Oxfordshire OX14 3DB, United Kingdom

(Received 24 August 2001; accepted 26 November 2001)

The transport of test particle ensembles moving in turbulent electrostatic fields governed by the Hasegawa–Mima equation is investigated. It ranges from subdiffusive to ballistic, depending on the size (in terms of thermal ion Larmor radii) of the domain considered, and on the magnitude of the background density gradient. In addition to the electrostatic potential, other fields, notably the vorticity and the Weiss field, prove to be very useful in accounting for particle dynamics and transport. For example, the existence of well defined core-circulation cell vortex structure in the Weiss field gives the most reliable guide to particle trapping, while locales of zero vorticity define regions of filamentary particle flow. Differential transport of guiding center particles and energetic particles gyrating with significant Larmor radius is investigated; the latter is strongly inhibited. © *2002 American Institute of Physics.* [DOI: 10.1063/1.1445426]

I. INTRODUCTION

The evidence for anomalous transport—that is, transport which is turbulence-driven and not necessarily describable by simple local diffusion—in magnetically confined plasmas is overwhelming. Classical reviews chronicling the development of observations, theory, and modelling over the past 15 years are provided by Refs. 1–4. In parallel, in a general physics context, interest has grown in the fundamental mechanisms that can give rise to anomalous transport, and in how they can be quantified and characterized; see, for example, Refs. 5–7. With some recent exceptions, however (see, for example, Refs. 8–10), there has been only a limited attempt to apply the general physics concepts of ''strange kinetics'' within a fusion context. In the present paper, we establish further linkages through a study of particle transport in strong plasma turbulence modelled by the Hasegawa–Mima (HM) equation,[11] whose physics is dominated by the $\mathbf{E}\times\mathbf{B}$ drift and involves low frequency (compared to the ion cyclotron frequency ω_{ci}) waves driven unstable by the presence of a density or temperature gradient. The Hasegawa–Mima equation thus provides a nonlinear model for drift turbulence in real space, whose output is the time dependent electrostatic potential. This potential then acts as an input for the equations of motion of ensembles of charged test particles, whose orbits we follow and whose statistical transport properties we then infer.

We have previously investigated radial particle transport in this way,[12,13] and found that nonlinear coupling significantly reduces the level of transport compared to the linear regime: this reduction was mainly ascribed to the formation of radial gradients in the velocity field. Now we turn to the poloidal component, and show that the HM model, despite its simplicity, yields evidence for transitions between qualitatively different types of transport when its parameters are varied. Poloidal plasma flow and poloidally extended turbulent structures are central to tokamak confinement, and interest has naturally focused on their implications for radial transport and confinement. Outward transport is the result of convolving poloidal and radial steps, and it is only safe to implicitly ''average over'' poloidal motion if one is convinced that: (a) the statistics of poloidal stepping are ''standard,'' so that one knows how to perform the poloidal averaging—this is not necessarily the case for non-Gaussian distributions; (b) poloidal and radial stepping are uncorrelated. Given the nature of turbulent transport (for example, the roles of trapping and jumps) and the (sometimes extreme) inhomogeneity of plasma turbulence in tokamaks, it appears worthwhile to explore the nature of poloidal transport in greater depth, so as to achieve progress on these questions. Further, as points (a) and (b) may depend on particle energy, we shall also investigate the impact of finite Larmor radius (FLR) effects on poloidal transport. We reported some preliminary results in a previous letter,[14] and in this paper we expand and explain them. We show how the vorticity and Weiss fields, derived from the electrostatic potential and described below, can be used to account for particle trapping and flights.

The HM equation[11] is a relatively simple two-dimensional model for the turbulent electrostatic field in the (x, y) plane perpendicular to the magnetic field ($\mathbf{B}\equiv B\hat{\mathbf{z}}$), and has many wider physical applications.[15] The model assumes cold ions, $T_i \ll T_e$ ($T_{i(e)}$ being the ion (electron) temperature), with negligible inertia parallel to $\mathbf{B}$. The quasineutrality con-

 © 2002 American Institute of Physics

Downloaded 27 Feb 2002 to 193.50.41.42. Redistribution subject to AIP license or copyright, see http://ojps.aip.org/pop/popcr.jsp

dition $n_i \simeq n_e$ is satisfied, where $n_{i(e)}$ is the ion (electron) density; the electrons are assumed to have an immediate adiabatic response, with Boltzmann distribution; and their background density depends only on y, equivalent to the radial direction in a tokamak, $n_0 \equiv n_0(y)$. The HM equation is then written[11–13]

$$\frac{\partial}{\partial t}(\phi - \nabla^2 \phi) - \{\phi, \nabla^2 \phi\} - \beta \frac{\partial \phi}{\partial x} = 0. \tag{1}$$

Here x and y are normalized to the thermal ion Larmor radius $\rho_s = c_s/\omega_{ci}$, where $c_s = \sqrt{T_e/m_i}$ is the sound speed and m_i the ion mass; the time t is normalized to L/c_s, where L is a characteristic length of the system; ϕ is the electrostatic potential normalized to $(T_e/e)(\rho_s/L)$; $\{A,B\} = \partial_x A\, \partial_y B - \partial_y A\, \partial_x B$ is the Poisson bracket and

$$\beta = \left| \frac{d}{dy} \ln[n_0(y)] \right| \tag{2}$$

is a parameter measuring the anisotropy of the background density (this should not be confused with the standard plasma β, the ratio of thermal to magnetic pressure). The linear limit of Eq. (1) is equivalent to the evolution of a collection of independent drift waves, each obeying the dimensionless dispersion relation

$$\omega_k = -\frac{\beta k_x}{1 + k^2}, \tag{3}$$

where $k_{x(y)}$ is the wave number in the $x(y)$ direction and $k^2 = k_x^2 + k_y^2$.

We have implemented[12,13] Eq. (1) in a computational box of area $L \times L$ (L is expressed in units of ρ_s), which is finite in the y direction and periodic in the direction of propagation of drift waves, x, which is equivalent to the poloidal direction in a tokamak. As explained previously,[12–14] for reasons of numerical stability a dissipation term D is added to the right hand side of Eq. (1) for high wave numbers, together with a forcing term S, in order to reach a quasistationary state. These terms have the following form in Fourier space:

$$D_k = -(\nu k^4)(1 + k^2)\phi_k, \quad S_k = A\, \delta(\mathbf{k} - \mathbf{k}_f), \tag{4}$$

where ν is the dissipation coefficient, while A and $\mathbf{k}_f$ are the amplitude and wave number of the forcing, which is localized at high wave numbers in both the x and y directions. The initial condition is taken to be a random distribution for the fluid part of the potential vorticity:

$$(\phi - \nabla^2 \phi)(x, y, t = 0) = \sum_n \sum_m \frac{A_0}{\sqrt{n^2 + m^2}} \sin\left[\frac{\pi}{L} m \left(y - \frac{L}{2}\right)\right] \times \cos\left(\frac{2\pi}{L} n x + \eta_{mn}\right), \tag{5}$$

where η_{mn} are random phases and A_0 is a constant. Equation (1) is solved numerically by means of a hybrid spline-spectral method coupled to a leapfrog integrator in time. Typically a mesh 512×513 is used.

The coefficient L represents the dimensions of the computational box, i.e., the number of thermal ion Larmor radii encompassed by it. The larger the box, the greater the number of vortices that it can support. This can qualitatively change the dynamics, as we shall see in Sec. III B. Furthermore, by varying the magnitude of the coefficient β in Eq. (1), one can control the importance of the linear terms, which arise from density anisotropy. The model is thus well suited to studying the linear dispersive effects of anisotropy on the poloidal transport of test particles (Sec. III C). Even for moderate values of β, the electrostatic potential develops an anisotropic spectrum, shallower in k_y and steeper in k_x.[16] This is a signature of the presence of zonal flows, i.e., potential structures elongated in the direction of propagation of drift waves (x), which are well known to have an impact on particle transport in the direction of the density gradient (y); see, for example, Refs. 12, 13.

The zonal flows considered in this paper are generated via the presence of linear dispersive waves (the so-called "β-effect"),[16] and are completely analogous to the zonal flows appearing in the context of geophysical fluid dynamics.[17] In tokamak physics, zonal flows can also be created by a different mechanism, which involves a nonadiabatic electron response for purely radial, zero-frequency modes. This requires a small (but significant) modification to the standard HM equation, as proposed by Smolyakov and co-workers.[18–22] In the present paper, we shall not consider this alternative route to zonal flow generation, but shall rather concentrate on the standard HM model. Zonal flow generation in the HM equation was also studied in a recent paper,[23] which includes the effect of magnetic shear.

The HM equation can also support drifting nonlinear vortex structures, which can trap particles for relatively long times, and therefore affect their diffusion rate. This effect has recently been studied by Naulin *et al.*,[24] who use a model similar to ours (the Hasegawa–Wakatani equations[25]), but with different boundary conditions, periodic in both directions. It appears that with such boundary conditions the effect of zonal flows is reduced. Particles are trapped within the vortices for some time, but ultimately they become untrapped, so that the computed diffusion[24] is approximately normal for both the radial and the poloidal directions. Finally, if a particle has finite Larmor radius, this can average out the smaller wavelengths that it experiences, thus affecting the transport; in Sec. IV we consider simulations that take this effect into account.

II. TEST PARTICLES

In order to analyze the transport of test particles moving in the HM field, we create an ensemble of 10^4 particles, seeded at rest once the turbulence has settled to a quasistationary state, and randomly distributed over the whole of the computational box except for a small border. Their subsequent motion is given by the $\mathbf{E} \times \mathbf{B}$ drift

$$\frac{d\mathbf{r}}{dt} = \mathbf{B} \times \frac{\nabla \phi}{B^2}. \tag{6}$$

Downloaded 27 Feb 2002 to 193.50.41.42. Redistribution subject to AIP license or copyright, see http://ojps.aip.org/pop/popcr.jsp

Here ϕ is the electrostatic potential resulting from the numerical solution of the HM equation and we neglect the polarization drift. The equations of motion are Hamiltonian in form, with the real space (x, y) coinciding with the phase space and $H(x,y,t)=\phi(x,y,t)/B$ as Hamiltonian. The test particles are noninteracting and without inertia, so that we consider only their guiding center motion; finite Larmor radius effects will be introduced later. Recall that for normal diffusion (a classical random walk), the mean squared displacement

$$\langle \Delta x^2 \rangle = \frac{\Sigma_{i=1}^{N}(x_i - \langle x \rangle)^2}{N}, \tag{7}$$

is proportional to time: $\langle \Delta x^2 \rangle \sim t$. If transport is anomalous ("strange kinetics" [5–7]), this becomes $\langle \Delta x^2 \rangle \sim t^{\mu}$: for $0<\mu<1$, we have subdiffusion; for $1<\mu<2$, supradiffusion; and for $\mu=2$, ballistic motion–particles move with constant velocity. The main purpose of the present paper is to evaluate the exponent μ for poloidal transport in turbulence governed by different regimes of the HM equation, and we shall see that μ can be smaller or larger than unity.

The equations of motion, Eq. (6), are solved numerically by means of a second order leapfrog scheme, which displays little numerical diffusion. The **E×B** velocity field at the particle locations is computed by linear interpolation. This overall numerical scheme has been tested by taking a "frozen" velocity field: in this case, the particles should simply rotate inside the vortices on closed orbits, with no diffusion. The scheme correctly reproduces this behavior, within good approximation, over a large number of rotations. L (the computational box dimension measured in units of ρ_s) and β (the anisotropy of the background density) are the two essential dimensionless parameters governing the HM equation. We have performed two sets of computer experiments: first, holding $\beta=0$ fixed (the isotropic and purely nonlinear case), we have run three simulations for different values of L; then, for $L=20$, we have run another set of simulations increasing the value of β.

III. TRANSPORT

A. Basic definitions

Let us briefly review some concepts that will assist in explaining some aspects of the transport. A two-dimensional turbulent field may be decomposed by distinguishing the contributions of rotation and deformation. In our case, the electrostatic potential ϕ is also acting as the stream function of the particles, in the sense that $\mathbf{v}\equiv(v_x, v_y)$ is the Eulerian velocity field

$$v_x = -\frac{\partial \phi}{\partial y}, \quad v_y = \frac{\partial \phi}{\partial x}. \tag{8}$$

Vortices with $\phi>0$ (<0) are called anticyclones (cyclones), and particles trapped in them rotate clockwise (anticlockwise). The vorticity w is

$$w = \frac{\partial v_y}{\partial x} - \frac{\partial v_x}{\partial y} = \nabla^2 \phi, \tag{9}$$

and the strain s is given by $s^2 = s_1^2 + s_2^2$, where

$$s_1 = \frac{\partial v_x}{\partial x} - \frac{\partial v_y}{\partial y} = -2\frac{\partial^2 \phi}{\partial x\, \partial y} \tag{10}$$

and

$$s_2 = \frac{\partial v_y}{\partial x} + \frac{\partial v_x}{\partial y} = \frac{\partial^2 \phi}{\partial x^2} - \frac{\partial^2 \phi}{\partial y^2}. \tag{11}$$

It is then possible to define the Weiss field Q by[26]

$$Q = s^2 - w^2. \tag{12}$$

As has been shown by Weiss,[26] if the strain rate along a particle path is slowly varying with respect to the vorticity gradient, the Lagrangian evolution of ∇w is given by a linear differential equation whose solution is

$$\nabla w \sim \exp(\pm \tfrac{1}{2}\sqrt{Q}\, t). \tag{13}$$

Thus Q determines whether, and how fast, two initially close fluid elements will (exponentially) separate ($Q>0$) or not ($Q<0$), following the frozen streamlines. The square root of Q is not a Lyapunov exponent in the strict mathematical sense, but plays an analogous role as an inverse timescale that quantifies the stochasticity of particle motion in the turbulent field.

One can therefore simplify the picture of two-dimensional turbulence by an elementary partitioning of the field into two distinct domains: elliptic domains ($Q<0$) where rotation dominates deformation, and hyperbolic domains ($Q>0$) where deformation dominates rotation. As pointed out, for example, by Elhmaïdi,[27] vortex cores with negative Q correspond to the center of the vortices in ϕ, and tend to be surrounded by an annular region of positive Q, called the circulation cell; in the following we will refer to this combination as a core-circulation cell vortex structure. These structures are usually embedded in a background sea where Q is close to zero and essentially random. They are normally more sharply spatially localized than vortices in ϕ, so that the Weiss field can give a clearer indication of the structures that dominate the field.

B. Uniform background density

To study the influence of the computational box dimensions on the transport of test particles, we have run the HM code for $\beta=0$ and increasing values of L, starting from $L=20$. Initial wave numbers are chosen with (n, m) in Eq. (5) in the ranges $4\leqslant n\leqslant 6$ and $8\leqslant m\leqslant 12$, and $A_0=2$. The particles are seeded once a stationary turbulent state has been reached, so the transport does not depend on the initial conditions of the HM field. The forcing is at high wave numbers, with amplitude $A=4$ in Eq. (4), and the dissipation coefficient ν is adjusted to the appropriate value for the scale considered. Unlike the Navier–Stokes equation, the HM equation contains a characteristic length scale, ρ_s, so that one can derive two estimates for the eddy turnover time (i.e., the typical timescale of the turbulence), for length scales smaller or larger than ρ_s. These are, respectively,

Downloaded 27 Feb 2002 to 193.50.41.42. Redistribution subject to AIP license or copyright, see http://ojps.aip.org/pop/popcr.jsp

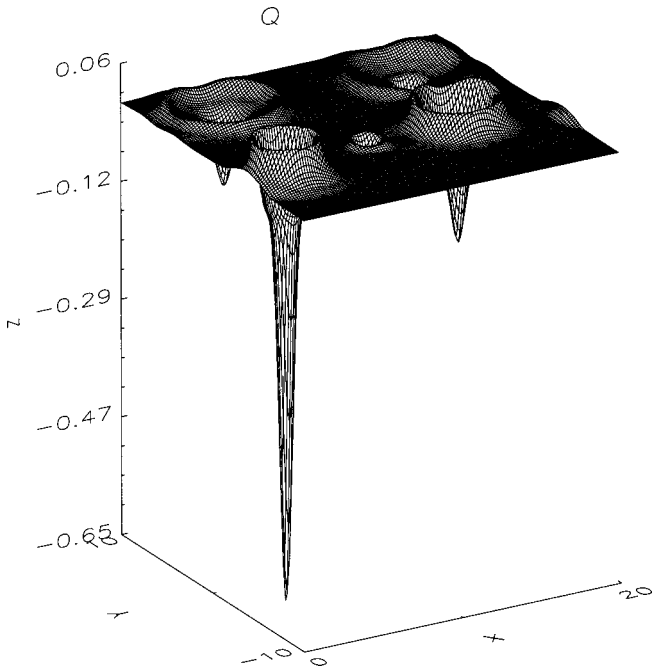

FIG. 1. Weiss field Q for $\beta=0$ and $L=20$, showing clear core-circulation cell vortex structures.

$$\tau_{es}=\left(\frac{1}{L^2}\int_L\int_L|\nabla^2\phi|^2\,d\mathbf{r}\right)^{-1/2};$$

$$\tau_{el}=\left(\frac{1}{L^2}\int_L\int_L|\nabla^4\phi|^2\,d\mathbf{r}\right)^{-1/2}; \tag{14}$$

all our simulations are run for several τ_{es} and τ_{el}.

For $L=20$, we take $\nu=6\times10^{-7}$ and $\mathbf{k}_f\simeq(40,40)$. Both τ_{el} and τ_{es} are of order unity, and our run lasts several hundreds of τ_e. The particles are seeded in the rectangle $1\leqslant x\leqslant19$ and $-9\leqslant y\leqslant9$. The electrostatic potential ϕ varies increasingly slowly as time evolves. After long times, four well-defined vortices in ϕ survive, and these correspond to four core-circulation cell vortex structures in the Weiss field Q, embedded in the background sea (Fig. 1). The core-circulation cell structure is extremely coherent, and evolves slowly on the turbulence timescale, while the background sea corresponds to very small Eulerian velocities. This is due to the fact that the vortices are too far from each other for their respective velocities to be additive; the velocities are much larger within the vortices than outside.

The test particles essentially follow the underlying vortex structure of the Weiss field Q, which, as we shall see, provides a more useful guide to their ensemble dynamics than does ϕ. Particles that start within a vortex core tend not to escape, even when two vortices merge, while particles that start outside a vortex core tend not to penetrate it. The vortex cores thus act as if surrounded by a nearly impermeable barrier.

From previous hydrodynamical simulations, Provenzale[28] points out that particles are ejected only during strong vortex–vortex interactions. In our case, even when two vortices merge into one, only a few particles are ejected, all the rest ending up in the resulting single vortex core.

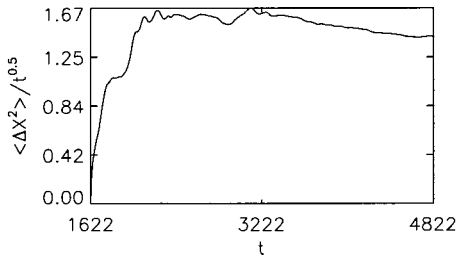

FIG. 2. Mean squared displacement $\langle\Delta x^2\rangle$ divided by $t^{0.5}$, for $\beta=0$ and $L=20$, showing quasisteady subdiffusion.

Provenzale also remarks that in forced turbulence, vortices are continuously generated (albeit slowly), and the only possibility for a particle to enter a vortex core is to be captured by a newly forming vortex during the generation process. Thus, in forced turbulence, the particle distribution becomes homogeneous on a very long timescale, which is determined by the typical lifetime of the vortices rather than by the eddy turnover time. In our particular case, the fields evolve very slowly, so the four vortices have a practically infinite lifetime. The resulting transport is clearly subdiffusive, as shown in Fig. 2, and the exponent μ tends slightly to decrease over time. This is due to the fact that the background velocity is very small and the vortices move increasingly slowly, partly because it is difficult to reach a perfectly stationary state in the simulation, so that the turbulence is slightly damped at long times.

For $L=120$ we take $\nu=3\times10^{-3}$ and $\mathbf{k}_f\simeq(6.5,6.5)$. The difference between $\tau_{es}\sim10$ and $\tau_{el}\sim300$ is now evident. We run the simulation for several tens of τ_{el} with the particles starting in the rectangle $10\leqslant x\leqslant110$ and $-50\leqslant y\leqslant50$. The Weiss field is shown in Fig. 3: in contrast to the previous case, no vortex structures are observed, and peaks and wells of Q have similar amplitudes, both several orders of magnitude smaller than in the $L=20$ case. This corresponds to a situation where only the randomly fluctuating background

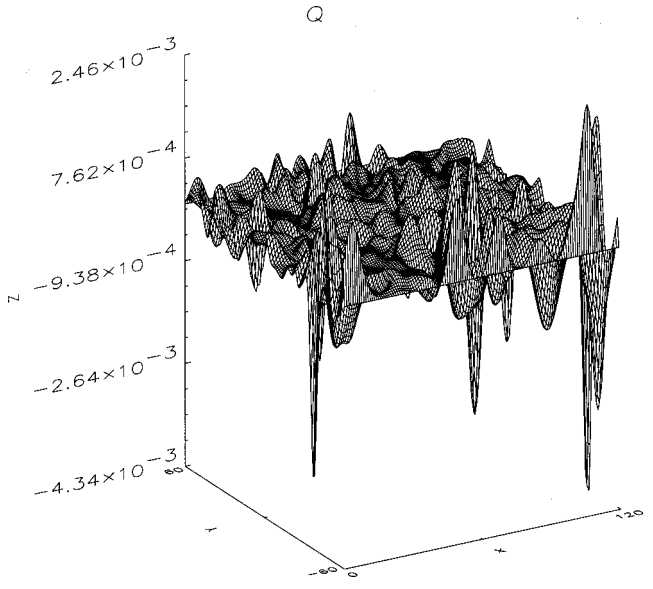

FIG. 3. Weiss field Q for $\beta=0$ and $L=120$: no vortex structures.

Downloaded 27 Feb 2002 to 193.50.41.42. Redistribution subject to AIP license or copyright, see http://ojps.aip.org/pop/popcr.jsp

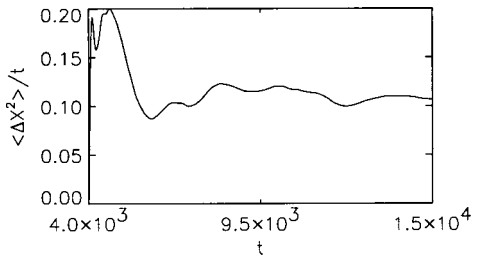

FIG. 4. Mean squared displacement $\langle \Delta x^2 \rangle$ divided by t, for $\beta=0$ and $L=120$, showing quasisteady normal diffusion.

sea is present. The Eulerian velocity displays some vortices, but is predominantly random. The particles still avoid some forbidden areas, but as a whole they are much more uniformly spread than for $L=20$. Their mean squared displacement (divided by time) is shown in Fig. 4, and is approximately constant, so that the resulting diffusion is normal.

For values of L between $L=20$ and $L=120$, the transport is subdiffusive, but with an exponent increasing with L, and the vortex structures are increasingly destroyed. Above $L=120$ the transport is normal and only the coefficient varies. We can make two deductions from those studies. First, the Weiss field plays the central role in determining particle trapping. Only if it corresponds to a core-circulation cell in the Q field does a vortex that is visible in the electrostatic field significantly trap particles and reduce the exponent of diffusion. Second, there is a well established transport regime (normal diffusion) once a threshold in L is crossed.

We also note that the vortices observed in Fig. 2 are reminiscent of the so-called Larichev–Reznik modon (see, for instance, Ref. 29 and references therein), which is an exact vortex solution to the HM equation propagating along the x direction. The modon is formed by a localized dipolar structure, with both potential and vorticity taking different signs on either sides of an axis of symmetry. This is, however, rather different from the vortices observed in our simulations, which display the core-circulation cell structure described above. Our vortices are spontaneously generated by the turbulence under the action of the forcing—they are not exact solutions of the HM equations, although they appear to survive over long times. Further, these vortex structures are no longer observed for larger values of L (Fig. 4).

In summary, we find that the particle transport changes nature with (restoring dimensional units) $L/\rho_s \equiv \rho_\star^{-1}$, where $\rho_\star$ is the normalized ion ''thermal'' Larmor radius. Transport scaling laws are sometimes expressed as $D \propto \rho_\star^\alpha$, where D is the transport coefficient and α an exponent defining the type of scaling (Bohm, gyro-Bohm, ...). Therefore, in our simulations, varying the dimensions of the computational box is equivalent to varying the value of $\rho_\star$. Our study shows that not only the scaling of the transport coefficient, but also the nature of the transport (normal versus ''strange''), can depend on the magnitude of $\rho_\star$. For moderate values of $\rho_\star$ $(=1/20)$, the observed transport is clearly subdiffusive. For smaller values ($\rho_\star \leqslant 1/120$, a regime more relevant to tokamak physics), the transport is normal, suggesting that the standard diffusion approximation can be justified in this context. This may not be the case, however, for small-size, low magnetic field laboratory devices operating at larger $\rho_\star$, for which the standard diffusion picture should be used with more caution.

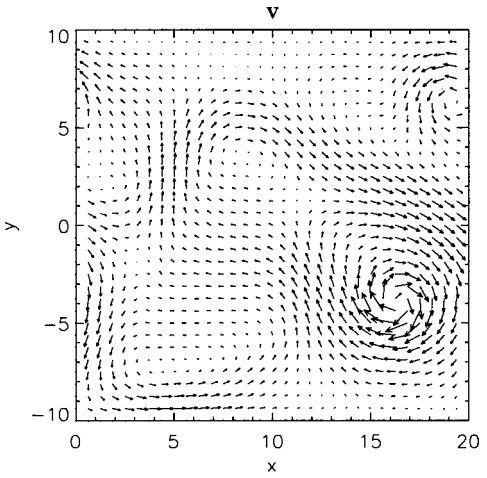

FIG. 5. Eulerian velocity field $\mathbf{v}$ for $\beta=0.05$ and $L=20$. Open paths from left to right are visible.

C. Increasing anisotropy

We turn now to the influence of density anisotropy (or, equivalently, of the linear term) in the HM equation. When β is increased, drift waves propagating toward the negative x direction appear. We therefore hold $L=20$ and run simulations with $\beta=0.05$ and $\beta=0.25$. The reference case is now the $\beta=0$ and $L=20$ simulation reported in Sec. III B; we use the same dissipation and forcing, obtaining approximately the same eddy turnover time. The initial position of the particles is the same as in the purely nonlinear case.

When $\beta=0.05$, the electrostatic potential ϕ displays two major vortices, but they are not as well defined and well separated as for $\beta=0$, and they move and merge much faster. Two vortex structures survive for long times and they drift in the $-x$ direction with a speed of the order of 10^{-2} in our units. Also, the Weiss field has elongated horizontal features, to which we will return later in this section. The Eulerian velocity field is displayed in Fig. 5, showing open paths from left to right, with rather high velocity.

The final positions of the test particles (Fig. 6) reveal ordered structures and display qualitatively different features on the left and on the right. At far left the particles are clustered in disks or circles, everywhere else being empty. The two disks are the vortices that were in the computational box at the time when the particles were injected. They have trapped the particles initially seeded in the cores and advected them. Analogously, the circulation cells have trapped some particles and are advecting them, explaining the circles of particles present. Figure 6(b) shows the portion $-150 \leqslant x \leqslant -90$ of the domain, with the particles superimposed on the Weiss field, and illustrates this phenomenon. The trajectory $x(t)$ of a trapped particle and the potential seen by it are displayed in Figs. 7(a), 7(b). It appears that the particle moves with constant velocity and stays on an isopotential curve within the vortex, so that the potential seen by the

Downloaded 27 Feb 2002 to 193.50.41.42. Redistribution subject to AIP license or copyright, see http://ojps.aip.org/pop/popcr.jsp

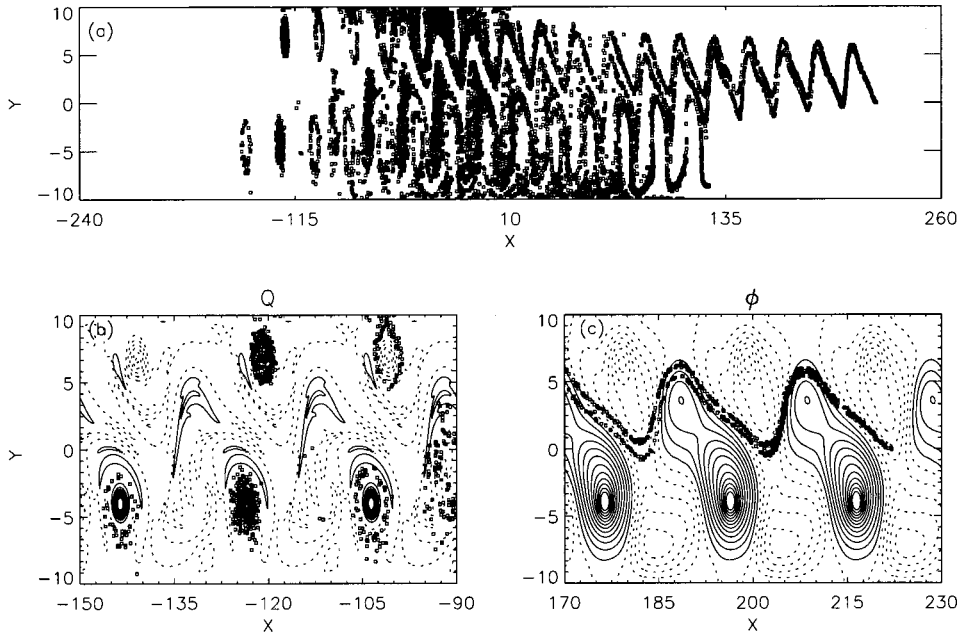

FIG. 6. Positions of the diffused test particles for $\beta=0.05$ and $L=20$. (a) Position of all the particles. (b) Particles at far left superimposed on the Q field. (c) Particles at far right superimposed on the ϕ field.

particle is approximately constant; the particle thus has ballistic motion at the speed of propagation of drift waves. The situation is different at far right, where we observe filaments of particles. These are located in the areas between neighboring vortices of opposite sign in ϕ, as is clear from Fig. 6(c), where the velocity of the two surrounding structures is additive, and there are open paths of Eulerian velocity. These particles have ballistic motion too, as can be deduced from the trajectory displayed in Fig. 7(c). However, the potential seen by these particles is not constant (as was the case for particles at far left), but rather oscillates around zero, as shown in Fig. 7(d). These oscillations are probably due to the random nature of the potential in the background sea between vortices. The remaining particles have less well defined types of motion: some perform random walks, while others are trapped in circulation cells and then advected to the left for a certain time. The coexistence of those different types of transport yields supradiffusion with exponent $\mu \sim 1.7$, as shown in Fig. 8.

For $\beta=0.25$, the vortices in the electrostatic potential ϕ propagate toward the left with a velocity of approximately 10^{-1}, which is an order of magnitude larger than for the case $\beta=0.05$. The field lines move and mix quickly, and no vortex survives for long times. The Weiss field displays no vortex structure, and only the background sea is left. The Eulerian velocity is much higher in the regions between electrostatic vortices than inside them, and there are open paths from left to right. Despite the apparent disorder of the ϕ and Q fields, the particles have closely correlated positions, as shown in Fig. 9. The fact that there are no longer

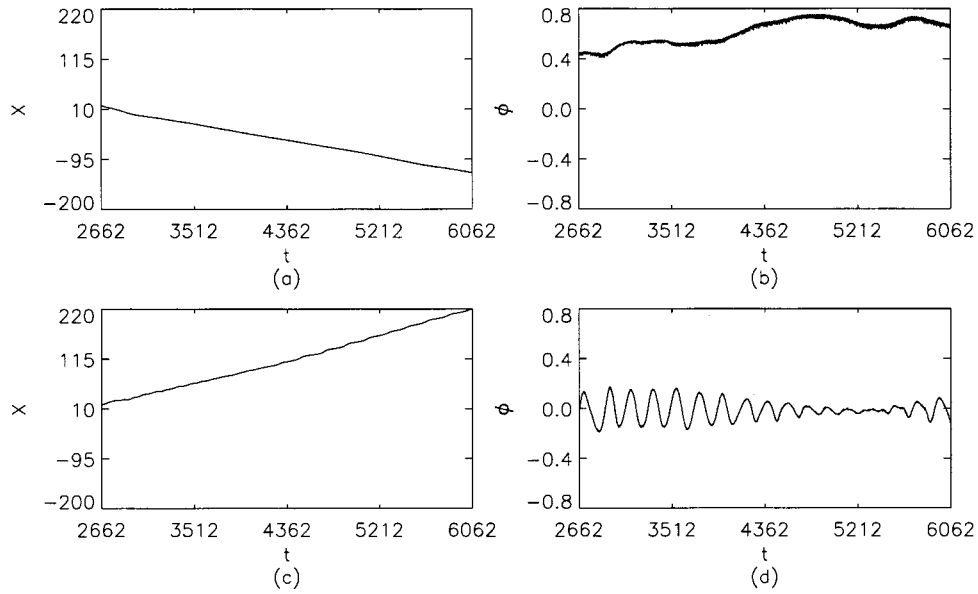

FIG. 7. (a) Trajectory $x(t)$ of a particle trapped by a vortex and (b) local potential at $x(t)$: the particle being trapped, ϕ is approximately constant and nonzero. (c) Trajectory $x(t)$ of a particle that travels to the far right and (d) local potential at $x(t)$: the particle oscillates across the region where ϕ changes sign. Parameters are $\beta=0.05$ and $L=20$.

Downloaded 27 Feb 2002 to 193.50.41.42. Redistribution subject to AIP license or copyright, see http://ojps.aip.org/pop/popcr.jsp

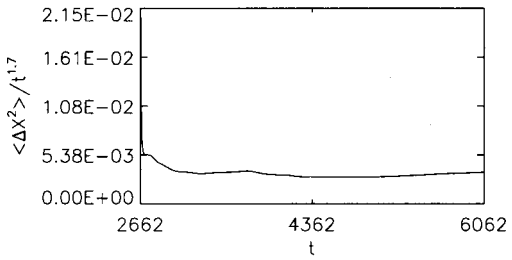

FIG. 8. Mean squared displacement $\langle \Delta x^2 \rangle$ divided by $t^{1.7}$, for $\beta = 0.05$ and $L = 20$, showing quasisteady supradiffusion.

any well defined structures in the Weiss field reduces the amount of trapping, and the best way of accounting for the position of the particles is now through the vorticity w, Eq. (9). Figure 10 shows a snapshot of w, displaying zonal flows (elongated structures) in the vorticity approximately parallel to the x axis. This is also reflected in the averaged correlation lengths of w, that in x being approximately double that in y. On the other hand, there is a tendency for the particles to stay in areas where $w \simeq 0$ (see also Ref. 27), so that the filaments of particles correspond to the isolines $w \simeq 0$ of the zonal flow. For example, the group of particles that travel to the far right follow the lower isoline $w = 0$ of the well defined pattern at $y \simeq -5$. There, the signs of the local vortices are such that the particles are pushed toward the right. Consideration of the vorticity field w is thus helpful in identifying dynamically significant zonal flows. These zonal flows are present throughout the duration of the run, and are responsible for the coherent particle positions displayed in Fig. 9. They also give rise to the layered pattern in Fig. 11, which shows how strongly the transport can depend on the initial position of the particles. This explanation also applies to the group of particles that travel to the far right in the case $\beta = 0.05$; see Fig. 6. The resultant transport is ballistic [Fig. 12(a)] and the mean displacement in x has increasing velocity toward positive x [see Fig. 12(b)], a feature known as "anomalous advection."[30] The influence of zonal flows and coherent structures, in a simple deterministic Hamiltonian model derived from the HM equation and incorporating asymmetric turbulence, has been studied by del Castillo–Negrete.[30,31] The author found that the trapping effect of the vortices combined with the zonal flows gives rise to anomalous diffusion, anomalous advection and Lévy statistics.

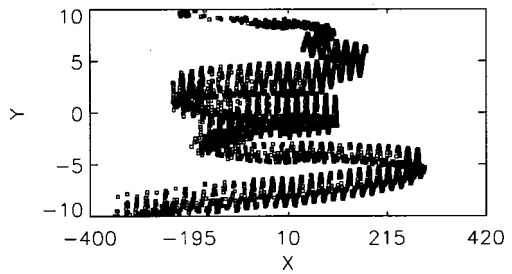

FIG. 9. Positions of the test particles for $\beta = 0.25$ and $L = 20$ at $t = 5482$, showing a high degree of spatial correlation.

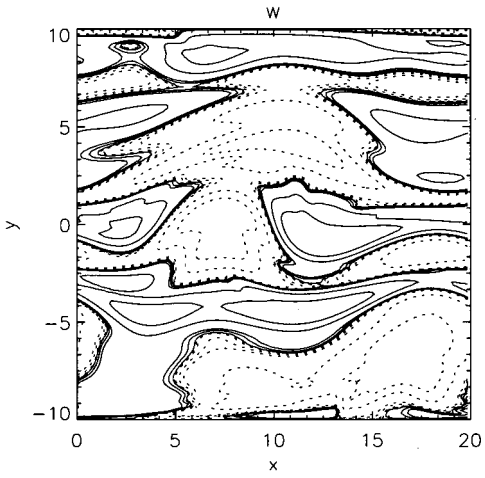

FIG. 10. Contour plot of the vorticity w for $\beta = 0.25$ and $L = 20$, showing zonal flows. Dotted lines: $w \leqslant 0$; unbroken lines: $w > 0$.

Other runs with $\beta > 0.25$ have been performed, all of which give ballistic motion with a coefficient increasing with β. As in the preceding subsection (Sec. III B), a well-established transport regime appears once a threshold in a specific parameter is crossed: in the present case the relevant parameter is β, and the threshold separates a region where the transport is supradiffusive from a region where it is ballistic. This threshold value of β decreases with increasing L because, in the HM equation, the relative importance of the nonlinear terms decreases for smaller wave numbers (and thus larger L). A schematic diagram of the types of poloidal transport resulting from the HM model when β and L are varied is displayed in Fig. 13.

IV. FINITE LARMOR RADIUS (FLR) EFFECTS

Fusion reactions in a deuterium-tritium tokamak palsma produce 3.5 MeV alpha particles whose Larmor radii greatly exceed those of the thermal ions, so that their response to

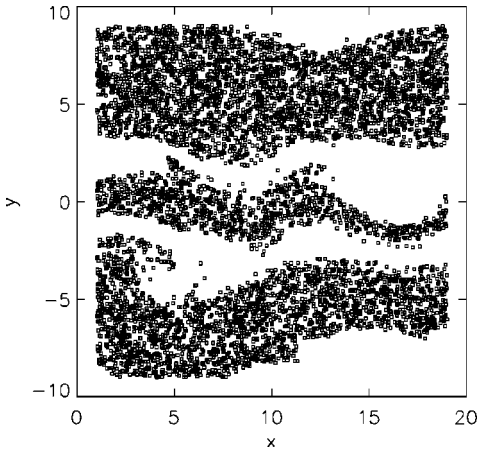

FIG. 11. Initial positions of the particles for which the total displacement in x is positive. Particles whose total displacement in x is negative have been removed. Case with $\beta = 0.25$ and $L = 20$.

Downloaded 27 Feb 2002 to 193.50.41.42. Redistribution subject to AIP license or copyright, see http://ojps.aip.org/pop/popcr.jsp

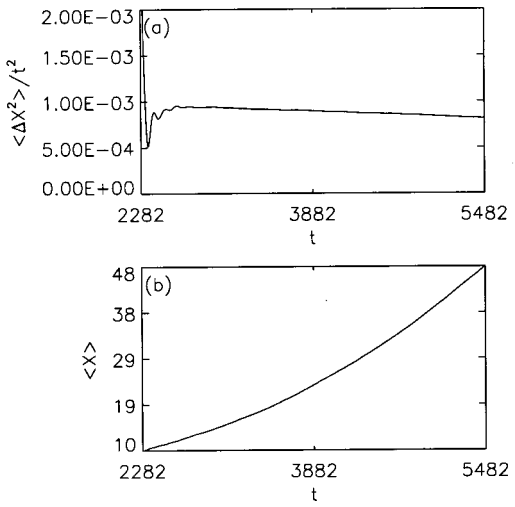

FIG. 12. Transport for $\beta=0.25$ and $L=20$. (a) Mean squared displacement $\langle \Delta x^2 \rangle$ divided by t^2, ballistic transport. (b) Mean displacement $\langle x \rangle$ increases with x, anomalous advection.

turbulence in the plasma can be significantly different. For example, the larger scale of gyromotion and drift motion will smooth out the effects of short wavelength turbulence, creating a differential response for particles of different energies. Given a theoretical understanding of this differential effect, observations of alpha particle transport may yield information on the characteristics of the turbulence. Studies of the influence of the finite Larmor radius (FLR) on the transport resulting from the linearized HM equation were performed in Refs. 12, 13, showing the reduction of the diffusion coefficient for increasing Larmor radii. Here we extend the simulations to the full equation.

The simplest model for FLR is obtained by 'spreading' the particle over a ring centered at the position of its guiding center, and this is accurate as long as the gyration frequency ω_{ci} is much larger than the drift frequency $\omega_* \simeq \omega_{ci}\rho_s/L_n$, where L_n is the typical density scale length. This model can be implemented numerically using linear interpolation to calculate the electric field at N_{gyro} (=8 in our case) points distributed over a ring whose radius is equal to the Larmor radius, and then averaging the electric field over those points.[32] The averaging operation tends to suppress the smaller scale components of the electric field.

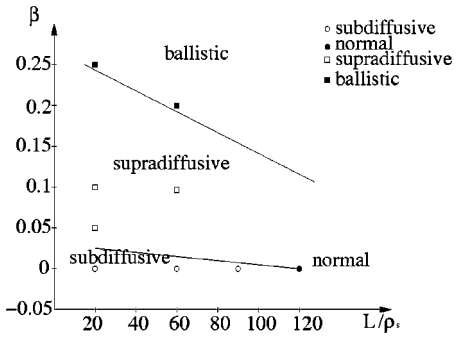

FIG. 13. Schematic of transport regimes in the parameter space (L,β). The squares and circles represent some of the runs; the lines separating the various regimes indicate approximately where the transitions occur.

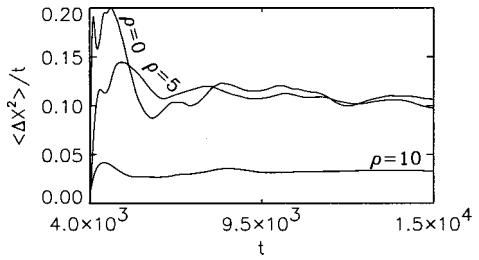

FIG. 14. Dependence of transport on Larmor radius for $\beta=0$ and $L=120$, for $\rho=0$, 5, and 10. Mean squared displacement $\langle \Delta x^2 \rangle$ divided by time reveals normal transport with diffusion coefficient decreasing with ρ.

Let us first consider runs with only nonlinear effects present, so that the fluctuations are isotropic. We take $L=120$, which gives normal diffusion. The fields are the same as in the analogous case of the preceding section, however, the 10^4 particles now have normalized Larmor radius $\rho=\rho_L/\rho_s$ (where $\rho_L=v_\perp/\omega_{ci}$) and start in a rectangle defined by $10\leqslant x\leqslant 110$ and $-50\leqslant y\leqslant 50$. When $\rho=1$ the transport is essentially identical to that obtained for $\rho=0$. Some small differences are visible when $\rho=5$, but for $\rho=10$ the diffusion coefficient is substantially reduced while the transport stays normal, as shown in Fig. 14. The correlation lengths for the electrostatic potential, λ_ϕ, the vorticity field, λ_w, and the Weiss field, λ_Q, have approximate values between 3 and 6, both in x and in y, with $\lambda_\phi \geqslant \lambda_w \geqslant \lambda_Q$ because $w\sim k^2\phi$ and $Q\sim k^4\phi$. Thus as long as ρ is smaller than or similar to the typical size of the structures, FLR effects are irrelevant. When ρ becomes larger, the averaging introduced by the FLR affects the particle response to the vortices, and the magnitude of the transport is greatly reduced, even though its qualitative character (normal) is unaltered.

For anisotropic fluctuations, we performed a run with $\beta=0.2$ and $L=60$, parameters which give ballistic motion when there are no FLR effects. We enlarged the computational box dimensions, because we require $\rho \ll L$, and for $\rho=0$, 1 and 5 we put 5000 particles in a rectangle defined by $10\leqslant x\leqslant 50$ and $-20\leqslant y\leqslant 20$. Figure 15 shows the resulting transport, which is evidently ballistic and again very similar for $\rho=0$ and $\rho=1$, whereas for $\rho=5$ it is strongly inhibited, although still ballistic. The reason for this threshold effect in the Larmor radius is to be found in the zonal flows, for which

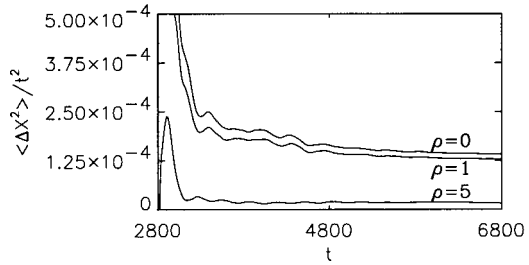

FIG. 15. Dependence of transport on Larmor radius for $\beta=0.2$ and $L=60$, for $\rho=0$, 1, and 5. Mean squared displacement $\langle \Delta x^2 \rangle$ divided by t^2 reveals ballistic transport with coefficient decreasing with ρ.

Downloaded 27 Feb 2002 to 193.50.41.42. Redistribution subject to AIP license or copyright, see http://ojps.aip.org/pop/popcr.jsp

the vorticity correlation length λ_w is ~ 5 in x and ~ 2.2 in y. When ρ is comparable to or larger than their width, the particle sees a field averaged over different uncorrelated vortices, so that the resultant velocity is strongly reduced.

We infer that the effect of FLR is negligible below a certain threshold, but when ρ becomes comparable to or larger than the turbulent structures that determine the transport, this strongly inhibits the diffusion. The value of the diffusion coefficient is then drastically reduced, while the exponent is relatively unaffected. FLR effects can thus create large quantitative changes in the transport, without changing its qualitative character.

V. CONCLUSIONS

We have performed numerical simulations of particle transport using the simplest model of strong two-dimensional electrostatic turbulence, the HM equation. When we fully take into account the nonlinear term in the equation, two parameters determine the character of the transport: the size of the computational box, and the anisotropy of the background density.

When the turbulence is isotropic or, equivalently, the HM equation is purely nonlinear, the transport in the (poloidal) x direction increases from subdiffusive, when the box dimensions are of the order of some tens of ρ_s, to normal, when the box dimensions are $120\rho_s$ or more. When the box dimensions are fixed to $20\rho_s$ and the anisotropy parameter β is increased, the transport rapidly becomes supradiffusive and, beyond a threshold at $\beta \approx 0.2$, ballistic. Particles follow qualitatively different trajectories (traps, jumps, etc.) depending on the control parameters of the turbulence and also on their different initial positions within a given simulation.

An important aspect that emerges from those results is the role of the Weiss field Q defined by Eq. (12) in determining particle trapping. When Q displays clear vortex structures, there is trapping and the transport depends on the motion of the structures. When there are no vortex structures in the Q field, there is no significant trapping, but even in this case the transport can be anomalous. In fact, the coherent patterns that can be observed in some cases (e.g., with nonzero β) can be due to zonal flows that are particularly visible in the vorticity field w, and are horizontally localized to regions where ϕ changes sign.

When the particles have a finite Larmor radius comparable to or bigger than the typical size of the structures dominating the transport in the flow, the diffusion is generally inhibited, in the sense that while the exponent does not greatly change, the coefficient is drastically reduced.

The results reported here, although derived from perhaps the simplest model that can be considered relevant to turbulent transport in tokamak plasmas, indicate the depth of complexity of the physical processes at work. They also confirm how strongly the transport depends on the control parameters. Nevertheless, there seems to be a general tendency to establish stable regimes once certain critical values of the dimensionless parameters β and L/ρ_s have been crossed. Our results also show how use of derived quantities, notably the vorticity and the Weiss potential, can assist in understanding some of the complexities of the underlying particle dynamics.

ACKNOWLEDGMENTS

We would like to thank Dr. J. J. Rasmussen and Dr. V. Naulin for useful discussions.

This work was supported in part by the U.K. Department of Trade and Industry and Euratom. S.V.A. is grateful for the support of a Marie Curie predoctoral fellowship awarded by the Commission of the European Communities (Contract no. 5004-CT97-5005).

[1] P. C. Liewer, Nucl. Fusion **25**, 543 (1985).
[2] W. Horton, Phys. Rep. **192**, 1 (1990).
[3] J. W. Connor and H. R. Wilson, Plasma Phys. Controlled Fusion **36**, 719 (1994).
[4] A. Yoshizawa, S.-I. Itoh, K. Itoh, and N. Yokoi, Plasma Phys. Controlled Fusion **43**, R1 (2001).
[5] M. F. Shlesinger, G. M. Zaslavsky, and J. Klafter, Nature (London) **363**, 31 (1993).
[6] G. M. Zaslavsky, D. Stevens, and H. Weitzner, Phys. Rev. E **48**, 1683 (1993).
[7] C. Tsallis, S. V. F. Levy, A. M. C. Souza, and R. Maynard, Phys. Rev. Lett. **75**, 3589 (1995).
[8] B. A. Carreras, B. van Milligen, M. A. Pedrosa *et al.*, Phys. Rev. Lett. **80**, 4438 (1998).
[9] G. M. Zaslavski, M. Edelman, H. Weitzner *et al.*, Phys. Plasmas **7**, 3691 (2000).
[10] G. Y. Antar, P. Devynck, X. Garbet, and S. C. Luckhardt, Phys. Plasmas **8**, 1612 (2001).
[11] A. Hasegawa and K. Mima, Phys. Fluids **21**, 87 (1978).
[12] G. Manfredi and R. O. Dendy, Phys. Rev. Lett. **76**, 4360 (1996).
[13] G. Manfredi and R. O. Dendy, Phys. Plasmas **4**, 628 (1997).
[14] S. V. Annibaldi, G. Manfredi, R. O. Dendy, and L. O'C. Drury, Plasma Phys. Controlled Fusion **42**, L13 (2000).
[15] A. Hasegawa, Adv. Phys. **34**, 1 (1985).
[16] G. Manfredi, J. Plasma Phys. **61**, 601 (1999).
[17] P. B. Rhines, J. Fluid Mech. **69**, 417 (1975).
[18] A. I. Smolyakov, P. H. Diamond, and M. Malkov, Phys. Rev. Lett. **84**, 491 (2000).
[19] A. I. Smolyakov, P. H. Diamond, and V. I. Shevchenko, Phys. Plasmas **7**, 1349 (2000).
[20] L. Chen, Z. Lin, and R. B. White, Phys. Plasmas **7**, 3129 (2000).
[21] P. N. Guzdar, R. G. Kleva, and L. Chen, Phys. Plasmas **8**, 459 (2001).
[22] G. Manfredi, C. M. Roach, and R. O. Dendy, Plasma Phys. Controlled Fusion **43**, 825 (2001).
[23] D. Jovanovic and P. K. Shukla, Phys. Lett. A **289**, 219 (2001).
[24] V. Naulin, A. H. Nielsen, and J. J. Rasmussen, Phys. Plasmas **6**, 4575 (1999).
[25] A. Hasegawa and M. Wakatani, Phys. Rev. Lett. **50**, 682 (1983).
[26] J. Weiss, Physica D **48**, 273 (1991).
[27] D. Elhmaïdi, A. Provenzale, and A. Babiano, J. Fluid Mech. **257**, 533 (1993).
[28] A. Provenzale, Annu. Rev. Fluid Mech. **31**, 55 (1999).
[29] D. Jovanovic and W. Horton, Phys. Fluids B **5**, 9 (1993).
[30] D. del-Castillo-Negrete, Phys. Fluids **10**, 576 (1998).
[31] D. del-Castillo-Negrete, Phys. Plasmas **7**, 1702 (2000).
[32] W. W. Lee, J. Comput. Phys. **72**, 243 (1987).

Downloaded 27 Feb 2002 to 193.50.41.42. Redistribution subject to AIP license or copyright, see http://ojps.aip.org/pop/popcr.jsp